Supporting Information for "Characteristics of slow slip events explained by rate-strengthening faults subject to periodic pore fluid pressure changes"

Andrea Perez-Silva[1], Yoshihiro Kaneko[2], Martha Savage[1], Laura Wallace[3,4]and Emily Warren-Smith[3]

[1]School of Geography, Environment and Earth Sciences, Victoria University of Wellington, PO Box 600, Wellington 6140, New Zealand.

[2]Department of Geophysics, Kyoto University, Sakyo-ku, Kyoto 606-8501, Japan.

[3]GNS Science, PO Box 30368, Lower Hutt 5011, New Zealand.

[4]Institute for Geophysics, University of Texas, Austin, Texas, USA.

Contents of this file

Additional Supporting Information (Files uploaded separately)

1. Movies S1 and S2

Introduction

The supporting text describes the elastodynamic equation that relates shear stress with fault slip (Text S1), the slip-rate doubling phenomenon (Text S2), alternative models with different r_0 under type II perturbation (Text S3) and the method to estimate stress drop (Text S4). Supporting figures illustrate the evolution of model variables for representative models shown in the main text (Figures S1 to S2), maximum slip of simulation cases in Figure 4 (Figure S3) and results from further parameter exploration (Figure S4). Examples of the slip-rate doubling phenomenon and models with different r_0 are shown in Figures S5 to S7 and Figures S8 to S9, respectively. Other aspects of modeled and observed SSE source properties are shown in Figures S10 and S11, respectively. We also provide reference tables presenting the model input parameters for simulation cases in the main text (Tables S1 and S3) and estimates of fault zone permeability based on the model results (Table S4). The supporting movies illustrate the evolution of the slip rate for representative models shown in the main text (Movies S1 and S2).

Text S1. Elastodynamic equation

Shear traction and fault slip are related through the following elastodynamic equation (Lapusta & Liu, 2009):

$$\tau(x,z;t) = \tau_0(x,z;t) + F(x,z;t) - \frac{\mu}{2c_s}V(x,z;t), \tag{1}$$

where $\tau_0(x,z;t)$ is the initial shear stress, μ is the shear modulus, c_s is the shear wave speed, $V(x,z;t)$ is the slip rate and $F(x,z;t)$ accounts for wave-mediated stress transfers. In our model, we assume a fully-dynamic approach, even though the slip rates are always below dynamic speeds.

Text S2. Slip-rate doubling

We term 'slip-rate doubling' the fault response characterized by SSE peak velocities that alternate between slow and fast values, which differ in several orders of magnitude (e.g., Figure S5). This response emerges under certain conditions for both perturbation types, as we describe in the following. Note that we do not include results of simulation cases with slip-rate doubling in the main text.

In exploring the perturbation parameters to reproduce Gisborne SSE properties (Figure 4), we find that large perturbations sometimes lead to slip-rate doubling. For type I case, perturbations with $R_0 \geq \sim$56 km ($R_0/L_b \geq 13.4$) induced SSEs with alternating slow and fast peak velocities (Figure S5a). The same behavior emerges in type II models for perturbations with $\sqrt{Dt_{\text{inj}}} \geq \sim$14 km ($\sqrt{Dt_{\text{inj}}}/L_b \geq \sim$3.36; Figure S5b).

For type II perturbation, slip-rate doubling emerged in two other cases: (1) After very sudden drops in pore-pressure during depressurization (i.e., $D_b \gg D$; cf. Figure S6a and S6b). (2) In simulation cases with short perturbation periods (1-2 yrs) and large size ($\sqrt{Dt_{\text{inj}}} \geq 13$ km, for $t_{\text{inj}} = 0.5$ yrs; e.g., Figure S7). The latter simulation cases were not included in Figure 5c.

We do not investigate the cause of slip-rate doubling, which is beyond the scope of this present study. However, it is likely related to the resonance behavior reported in the model of Perfettini et al. (2001) for velocity-weakening faults.

Text S3. Influence of r_0 on perturbation characteristics (type II) and SSE properties

In all simulations presented in the main text, $r_0 = 1$ km. To understand the changes in the perturbation characteristics with r_0, we explore different values of this parameter. To isolate the effect of r_0, we keep $\sqrt{Dt_{\text{inj}}}$ and $\Delta p_{\max}$ constant. Figure S8 shows the pore fluid pressure profiles (only during pore-pressure increase) for three perturbations cases with different r_0. We see that the width of the perturbation increases slightly with r_0 (Figure S8a). To keep $\sqrt{Dt_{\text{inj}}}$ and $\Delta p_{\max}$ constant, we apply a larger fluid flux when reducing r_0, which implies that the rate of pore-pressure increase is faster for cases with lower r_0 (Figure S8b).

To understand the role of r_0 on induced SSE properties, we impose perturbations with different r_0. Note that we adjust Δx to ensure that r_0 is well resolved in each case. For simplicity, we keep t_{inj} constant and explore different D. We calculate the average moment and duration of induced SSEs for each simulation case (Figure S9). For a given $\sqrt{Dt_{\text{inj}}}$, varying r_0 has a minor effect on induced SSE duration and moment. Likewise, SSE duration and moment do not correlate with changes in r_0 for a given $\sqrt{Dt_{\text{inj}}}$ (Figure S9).

Text S4. Estimating stress drop of induced SSEs

To estimate induced SSEs stress drop, we use the energy-based approach by Noda et al. (2013). In this approach, the stress drop $\overline{\Delta\sigma}_E$ is calculated by averaging the stress drop distribution with the actual final slip at each point as the weighting function (Noda et al., 2013):

$$\overline{\Delta\sigma}_E = \frac{\int_{\sum} \Delta\sigma \, \Delta u \, dS}{\int_{\sum} \Delta u \, dS} \tag{2}$$

where S is the SSE source area, $\Delta\sigma$ is the initial shear stress minus the final shear stress at each ruptured location and Δu is the final slip distribution of the SSE. The SSE source area is defined as the region with slip greater than the minimum slip = 1.1 $\times V_{pl}$ $\times$SSE duration (Section 4.1).

Movie S1 and S2. The movies show the slip rate evolution on the fault during induced SSEs from the representative models of shallow Gisborne SSEs under type I (Movie S1) and II (Movie S2) perturbations (Figures 2 and 3). A description of the fault response for each model is given in Section 3.1.

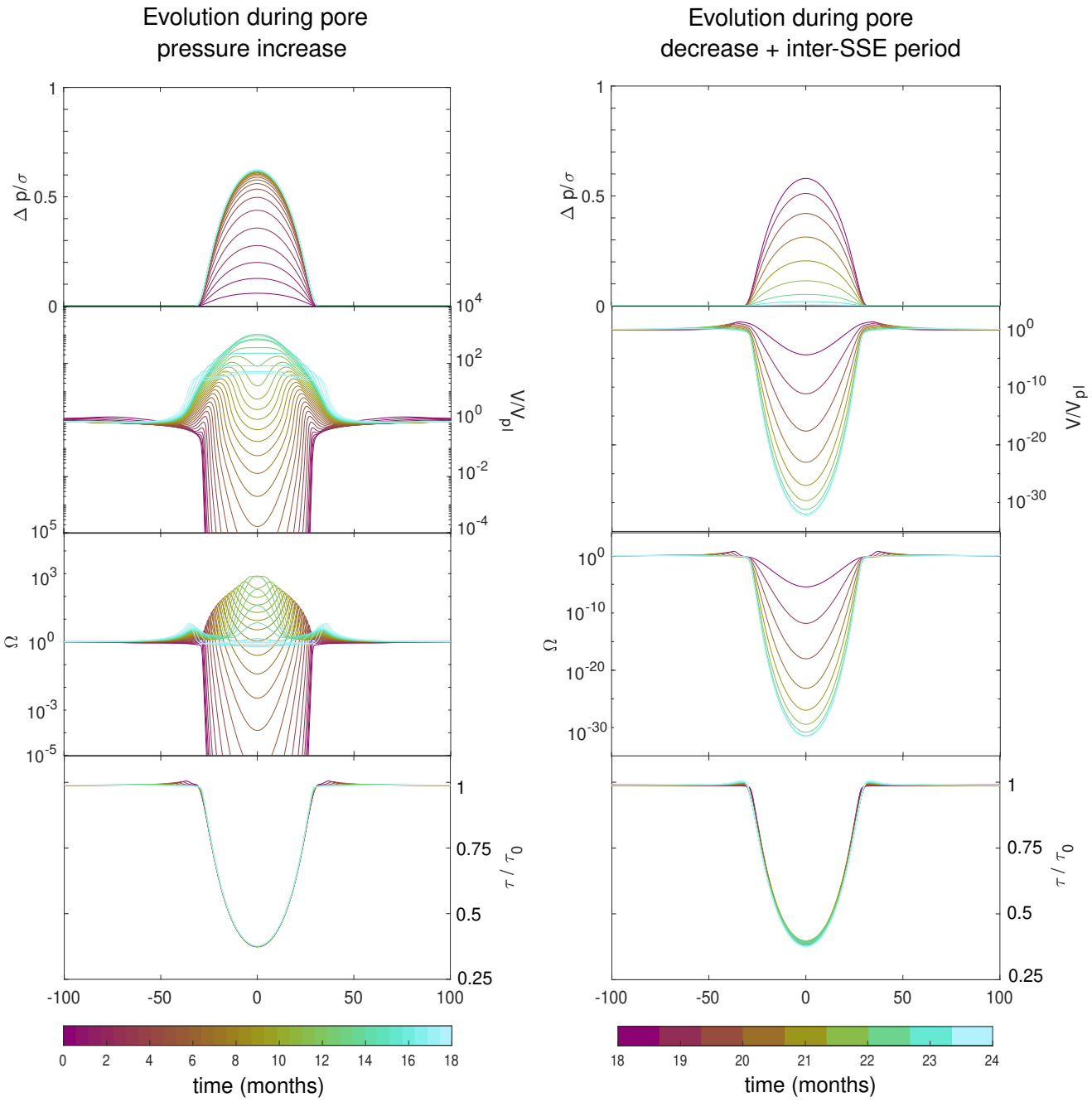

Figure S1. Temporal and spatial evolution of several terms during an induced SSE. Ω represents the distance to steady state $\Omega = \frac{V\theta}{d_c}$ (Rubin & Ampuero, 2005) and τ_o the initial shear stress. Results correspond to the representative model under type I perturbation (Figure 2).

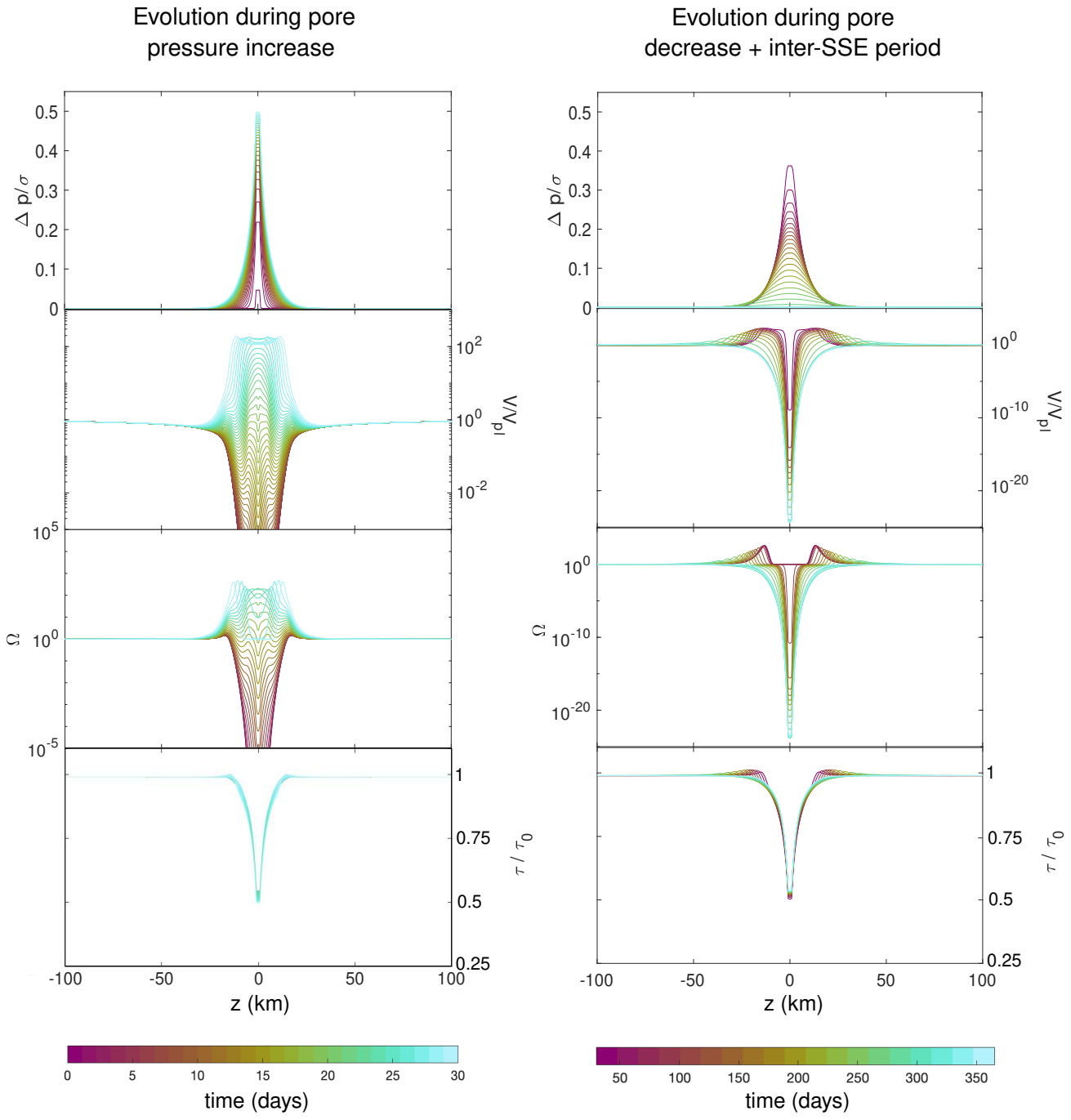

Figure S2. Temporal and spatial evolution of several terms during an induced SSE. Ω represents the distance to steady state $\Omega = \frac{V\theta}{d_c}$ (Rubin & Ampuero, 2005) and τ_o the initial shear stress. Results correspond to the representative model for type II perturbation (Figure 3).

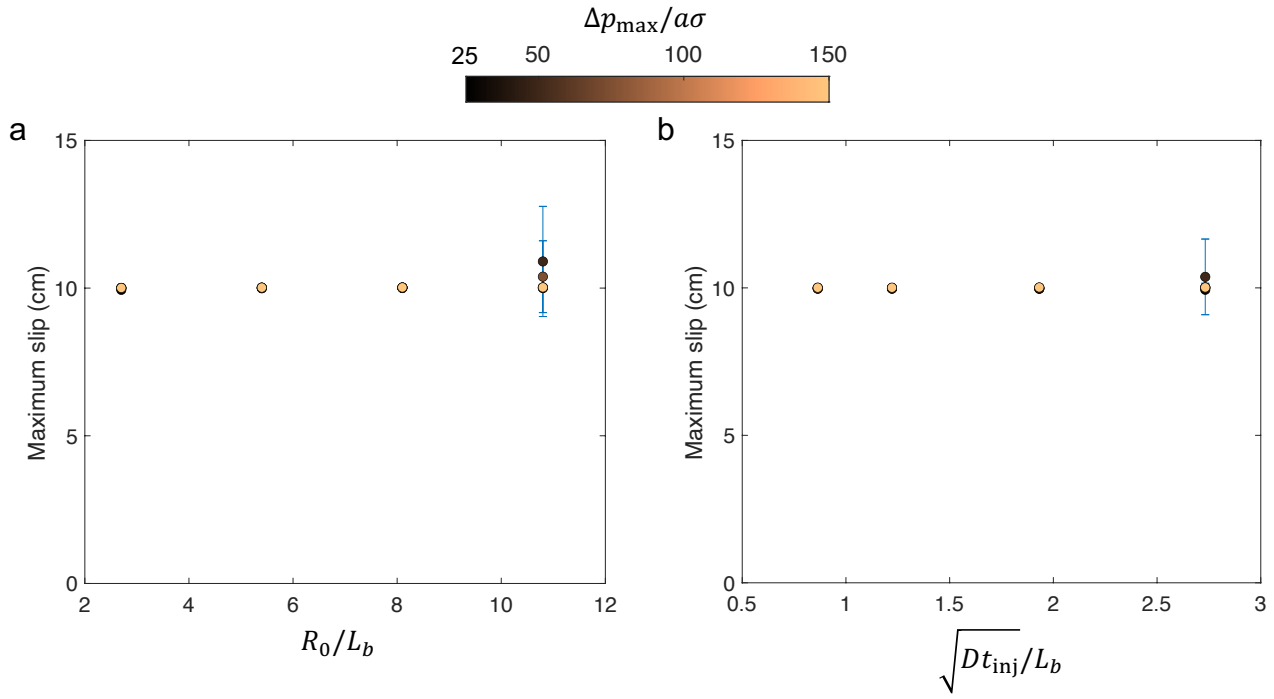

Figure S3. Average maximum slip of SSEs induced by periodic perturbations in pore pressure of (a) type I and (b) type II shown as a function of the characteristic size of the perturbation. Maximum slip is ∼10 cm in all cases. Results correspond to the parameter exploration shown in Figure 4. Vertical lines show standard deviation.

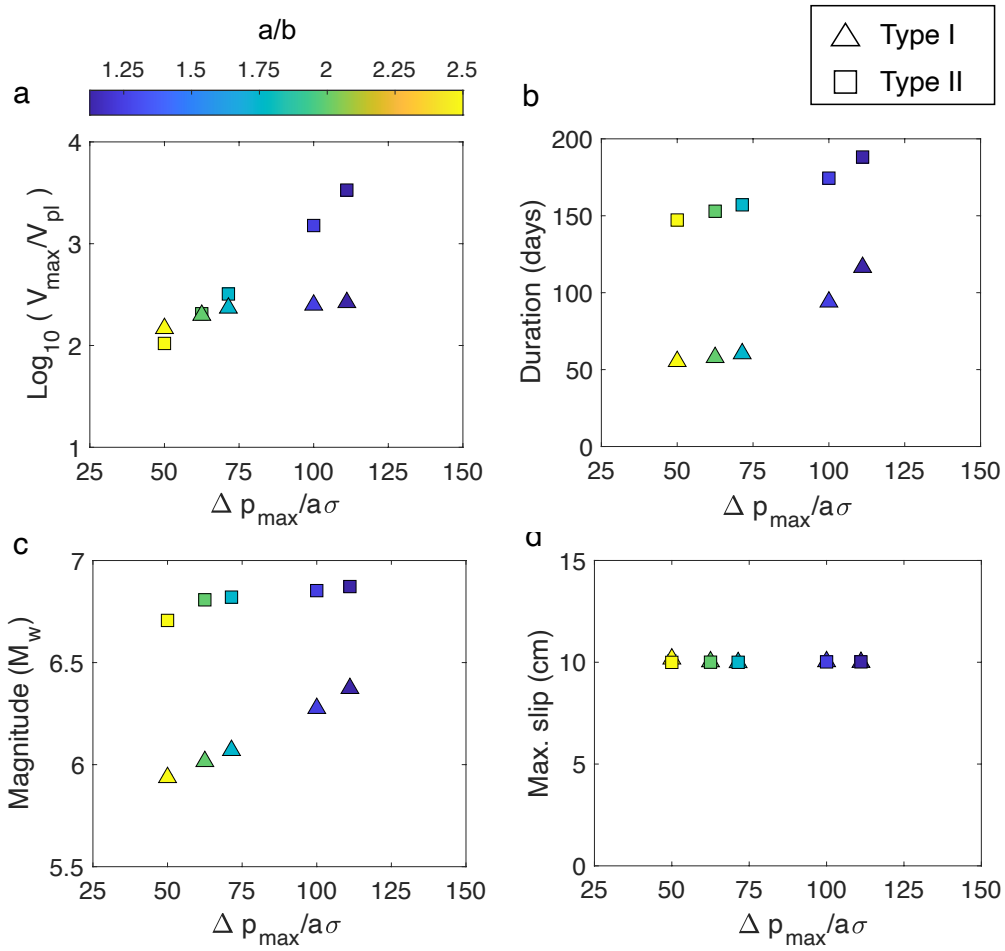

Figure S4. Exploration of a/b, a ranges from 0.0044 to 0.01 and $b = 0.004$. Average SSE properties: (a) maximum slip rate, (b) duration, (c) magnitude (M_w), and (d) max. Slip, are shown as a function of perturbation amplitude for type I (triangles) and type II (squares) perturbation. The amplitude of the perturbation is $\Delta p_{max} = 1.88$ MPa (type I) and 1.5 MPa (type II). The size of perturbation is equivalent to those of the representative models for type I and type II perturbation (Table 2). Average SSE properties (a-c) increase with the perturbation amplitude or equivalently in this case, decrease with a/b. The maximum slip remains constant ($\sim$10 cm). Note that we set V_{thr} to 0.3 mm/day to calculate SSE properties (Section 4.1).

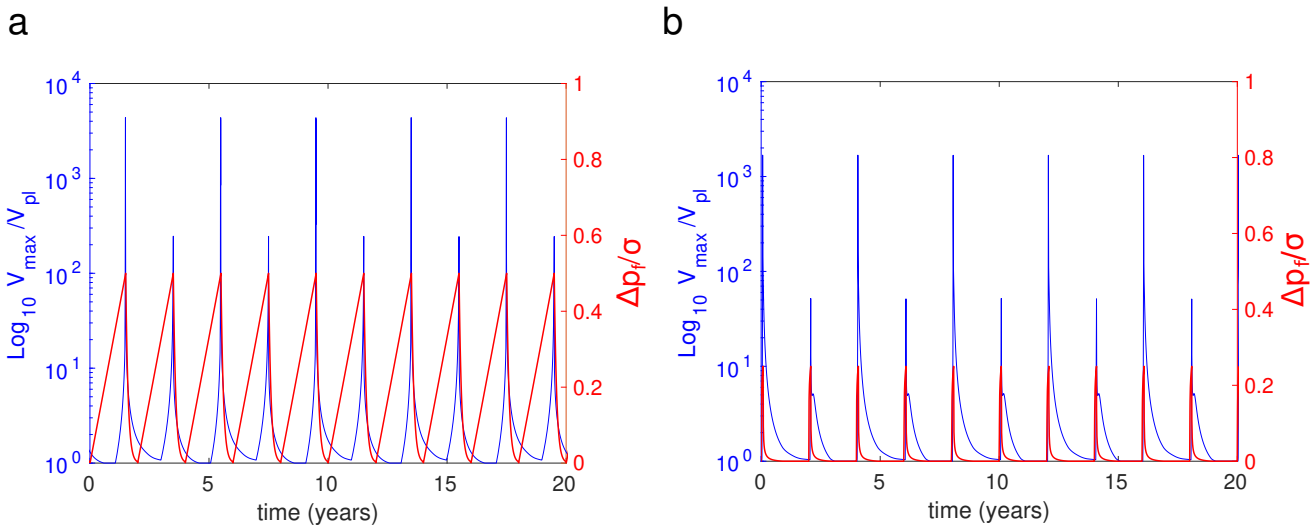

Figure S5. Temporal evolution of $V_{\max}/V_{\rm pl}$ (blue line) and $\Delta p_{\rm f}/a\sigma$ at the fault center (red line) for simulation case under (a) type I perturbation with $\Delta p_{\max}/a\sigma$=100 and R_0/L_b=13.5 (R_0=56.25 km) and (b) type II perturbation with $\Delta p_{\max}/a\sigma$=75 and $\sqrt{Dt_{\rm inj}}/L_b$=2.74 ($\sqrt{Dt_{\rm inj}}$=11.4 km). SSE peak velocity alternates between a slow and fast value, a behavior we refer to as 'slip-rate doubling' (Text S2). Model parameters are as given for shallow Hikurangi SSEs (Table 1).

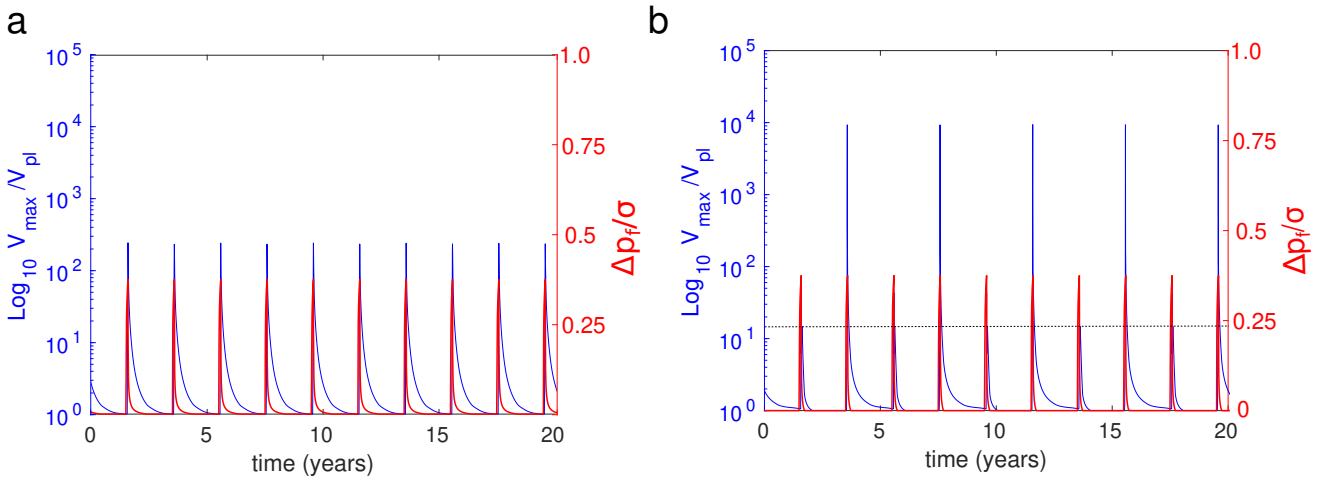

Figure S6. Temporal evolution of $V_{\max}/V_{\rm pl}$ (blue line) and $\Delta p_{\rm f}/a\sigma$ at the fault center (red line) with respect to time for simulation case under type II perturbation with $\sqrt{Dt_{\rm inj}}/L_b = 2.74$ (with $D = 50$ m^2/s and $t_{\rm inj} = 30$ days) and $\Delta p_{\max}/a\sigma$= 75. Example cases with different D_b. (a) $D_b = 55$ m^2/s and (b) $D_b = 75$ m^2/s. Dashed black line in (b) indicates the peak velocity of the slow-velocity SSE. Slip-rate doubling emerges in simulation with largest D_b (Text S2). Model parameters are as given for shallow Hikurangi SSEs (Table 1).

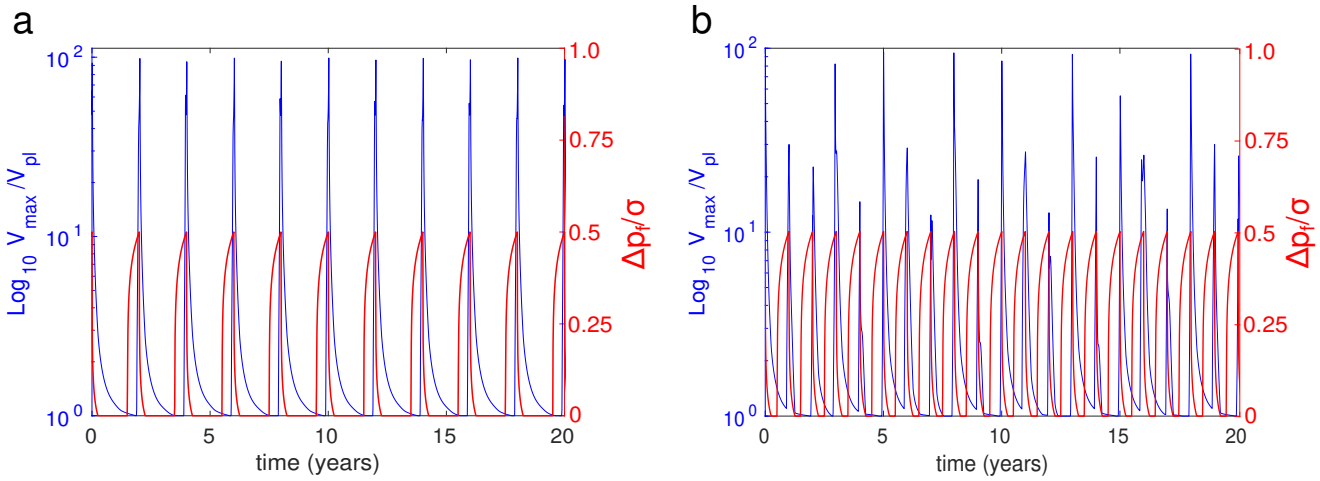

Figure S7. Temporal evolution of $V_{\max}/V_{\rm pl}$ (blue line) and $\Delta p_{\rm f}/a\sigma$ at the fault center (red line) with respect time for simulation case under type II perturbation with $\sqrt{Dt_{\rm inj}}/L_b \sim 3$ and $\Delta p_{\max}/a\sigma = 100$. Simulation cases with different perturbation period: (a) 2 yrs and (b) 1 yr. Slip-rate doubling effect arises in simulation case with shorter perturbation period (Text S2). Model parameters are as given for Figure 5c (Table 1).

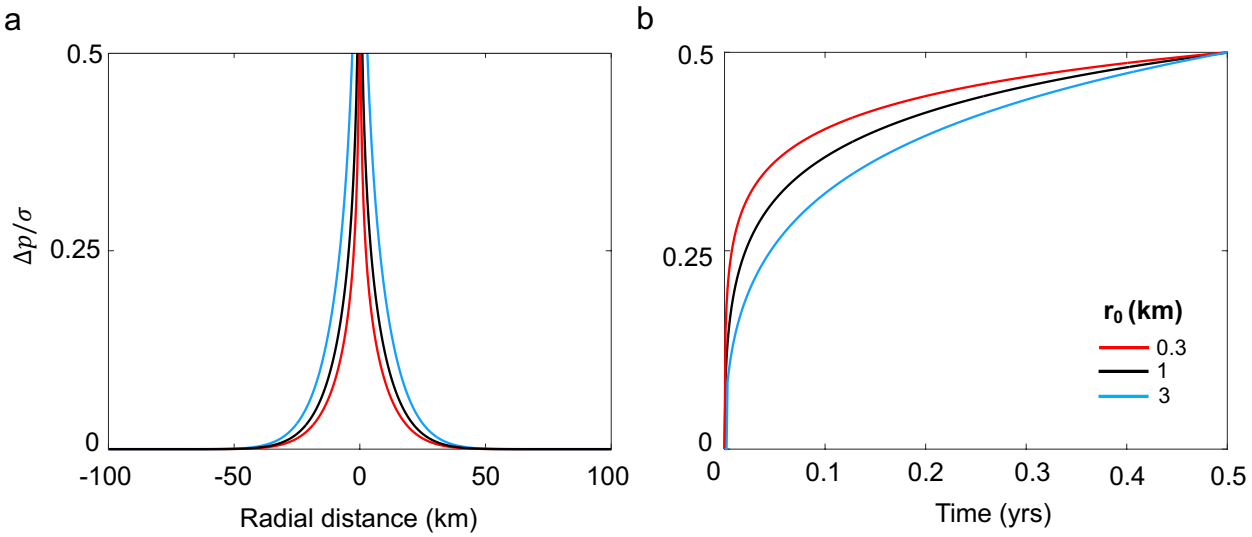

Figure S8. Pore fluid pressure evolution for simulations with constant $\sqrt{Dt_{\text{inj}}}$ (= 12.6 km) and Δp_{max} (= 4.5 MPa, for σ = 9 MPa), but different r_0. (a) Pore-pressure profiles with respect fo the radial distance at t_{inj} = 0.5 yrs. (b) Pore-pressure evolution with respect to time.

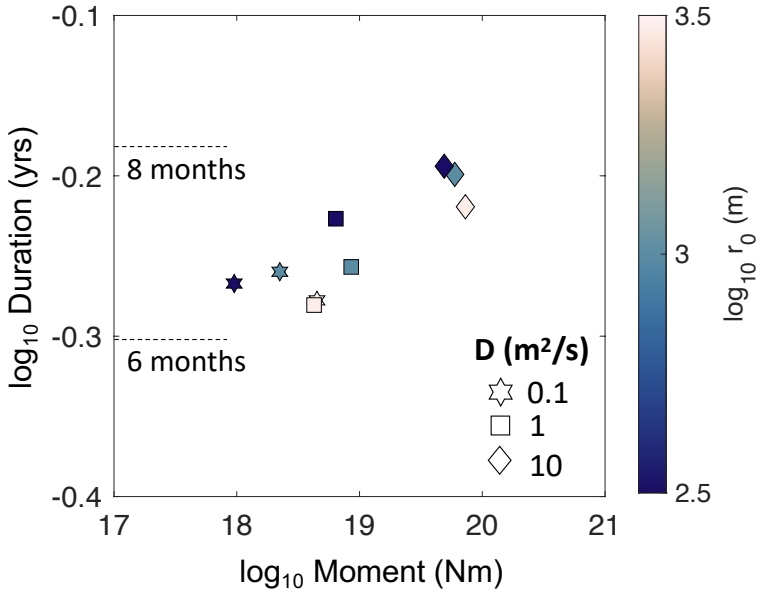

Figure S9. Exploration of r_0 in simulation cases with constant t_{inj} = 0.5 yrs and different D. Average moment and duration of induced SSEs with respect to r_0. $\Delta p_{\text{max}}/a\sigma$= 0.5 in all cases. Model parameters are given in Section 5.1.

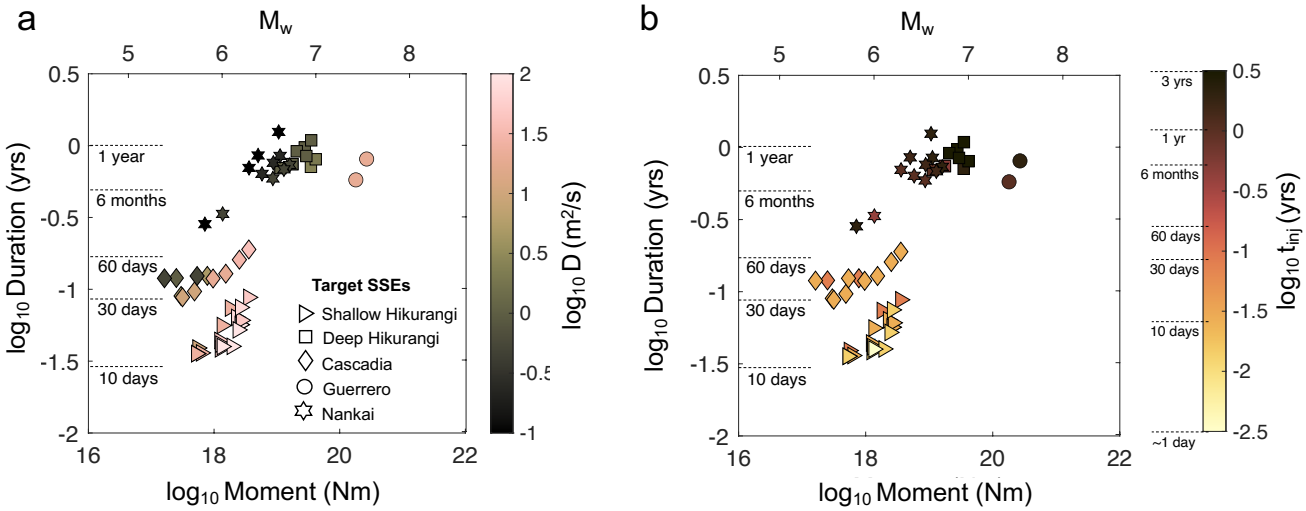

Figure S10. Average duration and moment of modeled SSEs induced by type II perturbations. Simulation cases are the same as in Figure 6b. For each simulation case, the corresponding (a) D and (b) t_{inj} are shown.

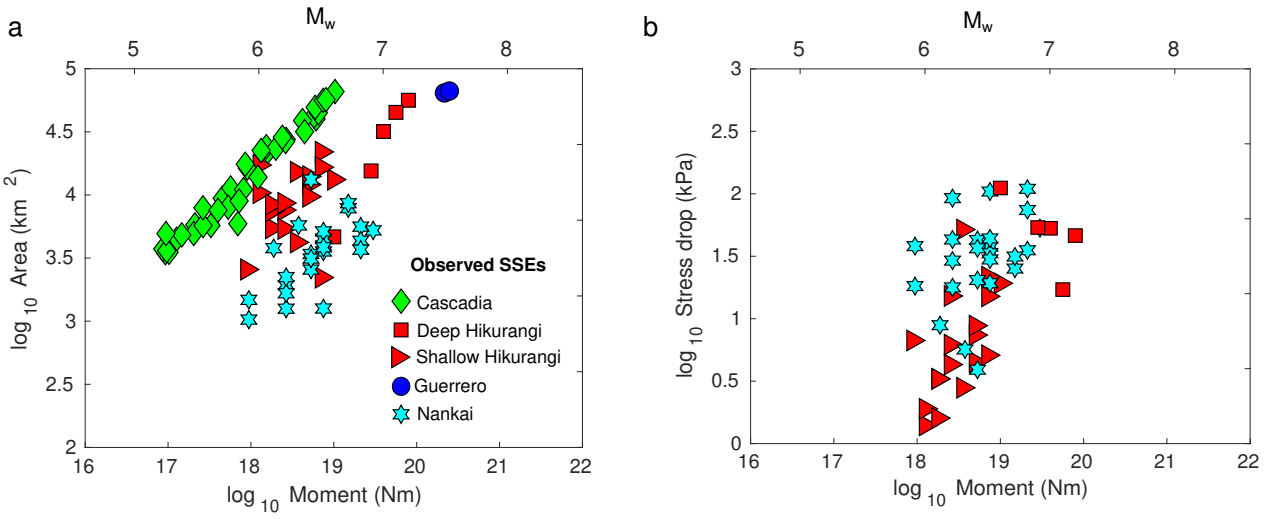

Figure S11. Source properties of observed SSEs from Cascadia (Michel et al., 2019), deep and shallow Hikurangi (Ikari et al., 2020), Guerrero (Radiguet et al., 2012) and Nankai (Takagi et al., 2019) subduction zones. (a) Moment-Area. (b) Moment-stress drop. Note that only stress drops from Nankai and Hikurangi SSEs were constrained by observations. To define the stress drop of Deep Hikurangi SSEs from Ikari's (2020) catalog, we calculated the average stress drop between the different stages of each event.

Table S1. Range of parameters explored for shallow Gisborne SSEs in Section 4.

	Parameter	Symbol	Range explored
Type I	Maximum pore pressure change	$\Delta p_{\max}$	0.375 - 2.25 MPa
	Normalized pore pressure change	$\Delta p_{\max}/a\sigma$	25 - 150
	Perturbation radius	R_o	11.25 - 45 km
	Normalised perturbation radius	R_o/L_b	2.7 - 10.8
Type II	Maximum pore pressure change	$\Delta p_{\max}$	0.375 - 2.25 MPa
	Normalised pore pressure change	$\Delta p_{\max}/a\sigma$	25 - 150
	Hydraulic diffusivity	D	5 - 50 m^2/s
	Injection time	$t_{\text{inj}}^{\text{a}}$	30 days
	Normalised perturbation size	$\sqrt{Dt_{\text{inj}}}/L_b$	0.8 - 2.8

[a]Note that we consider other t_{inj} for shallow Hikurangi SSEs in Figure 6 (Table S3)

Table S2. Perturbation characteristics of simulation cases shown in Figures 5a. For all cases $\Delta p_{\max}/\sigma = 0.5$, where $\sigma = 9$ MPa.

D (m^2/s)	D_b (m^2/s)	t_{inj}	$\log_{10}\sqrt{Dt_{\text{inj}}}/L_b$
0.1	0.3	2 yrs	-0.22
		1 yr	-0.37
		0.5 yr	-0.52
		30 days	-0.91
		10 days	-1.15
1	3	2 yrs	0.28
		1 yr	0.13
		0.5 yr	-0.02
		30 days	-0.41
		10 days	-0.65
10	30	2 yrs	0.78
		1 yr	0.63
		0.5 yr	0.48
		30 days	0.09
		10 days	-0.15
100	150[a]	1 yr	1.13
		0.5 yr	0.98
		30 days	0.59
		10 days	0.35

[a]Note that $D_b/D = 1.5$ (instead of 3) for $D = 100$ m^2/s, as larger D_b led to slip-rate doubling (Text S2)

Table S3. Perturbation characteristics of simulation cases shown in Figure 6b to 6d.

Target SSEs	D (m^2/s)	D_b (m^2/s)	t_{inj}	$\log_{10}\sqrt{Dt_{inj}}/L_b$	$\Delta p/a\sigma$	T_{per} (yrs)
Shallow Hikurangi	10	50	30 days	0.09	0.5	2
	25	40	30 days	0.29	0.5	2
	25	40	10 days	0.05	0.5	2
	25	40	10 day	0.05	0.5	5[(a)]
	25	40	5 days	-0.1	0.5	5
	50	75	30 days	0.44	0.5	5
	50	75	10 days	0.2	0.5	2
	50	75	10 days	0.2	0.5	2
	50	75	5 days	0.05	0.5	5
	60	85	5 days	0.09	0.5	5
	75	90	5 days	0.29	0.5	2
	75	80	5 days	0.14	0.5	5
	100	90	10 days	0.35	0.5	5
	100	130	10 days	0.35	0.5	2
	100	125	5 days	0.2	0.5	5
	100	150	5 days	0.2	0.5	5
	100	125	1 day	-0.15	0.5	5
Deep Hikurangi	1	2	2 yrs	0.28	0.5	5
	1	2	1 yr	0.13	0.5	5
	1	2	0.5 yr	-0.02	0.5	5
	1	4	3 yrs	0.37	0.5	5
	1	2	3 yrs	0.37	0.5	5
	1	6	4 yrs	0.43	0.5	5
	1	4	3 yrs	0.37	0.75	5
	2	7	3 yrs	0.52	0.5	5
	2.5	5	2 yrs	0.48	0.5	5
Cascadia	1	3	30 days	-0.41	0.5	1.5
	0.5	1.5	10 days	-0.8	0.5	1.5
	0.5	1.5	10 days	-0.8	0.5	1.5
	5	15	10 days	-0.3	0.5	1.5
	5	15	30 days	-0.07	0.5	1.5
	10	30	10 days	-0.15	0.5	1.5
	10	30	10 days	-0.15	0.25	1.5
	20	25	10 days	0	0.5	1.5
	20	25	10 days	0	0.25	1.5
	30	35	10 days	0.09	0.5	1.5
	40	45	10 days	0.15	0.5	1.5
Nankai	0.1	0.5	2 yrs	-0.22	0.5	6
	0.1	0.5	2 yrs	-0.22	0.5	3
	0.1	0.5	1.5 yrs	-0.28	0.5	3
	0.1	0.5	1 yr	-0.37	0.5	3
	0.25	1.5	2 yrs	-0.02	0.5	3
	0.25	1.5	1.5 yr	-0.08	0.5	3
	0.25	1.5	1 yr	-0.17	0.5	3
	0.5	2	2 yrs	0.13	0.5	3
	0.5	2	1.5 yr	0.07	0.5	3
	0.5	2	1 yr	-0.02	0.5	3
	0.5	2	0.4 yr	-0.22	0.5	3
Mexico	20	40	2 yrs	0.93	0.5	4
	20	40	1 yr	0.78	0.5	4

[a]Shallow Hikurangi SSEs in the southern part of the margin have recurrence time of ∼5 yrs, therefore we set T_{per} to 5 yrs (Wallace, 2020).

Table S4. Estimation of fault zone permeability (k) through the relation $k = D\eta\beta\phi$, assuming uniform η=10^{-3} Pa·s (fluid viscosity), $\beta = 10^{-8}$ Pa^{-1} (effective compressibility) and $\phi = 0.05$ (porosity). We set the same hydraulic diffusivity (D) required to reproduce SSE duration and magnitude with our model (Figure S10a and Table S3).

Target SSEs	D **(m^2/s)**	$k = D\eta\beta\phi$ **(m^2)**
Shallow Hikurangi	10	5E-12
	25	1.25E-11
	50	2.5E-11
	60	3E-11
	75	3.75E-11
	100	5E-11
Deep Hikurangi	1	5E-13
	2	1E-12
	2.5	1.25E-12
Cascadia	1	5E-13
	0.5	2.5E-13
	5	2.5E-12
	10	5E-12
	20	1E-11
	30	1.5E-11
	40	2E-11
Nankai	0.1	5E-14
	0.25	1.25E-13
	0.5	2.5E-13
Guerrero	20	1E-11

References

Ikari, M. J., Wallace, L. M., Rabinowitz, H. S., Savage, H. M., Hamling, I. J., & Kopf, A. J. (2020). Observations of laboratory and natural slow slip events: Hikurangi subduction zone, New Zealand. *Geochemistry, Geophysics, Geosystems*, *21*(2), e2019GC008717. doi: 10.1029/2019GC008717.

Lapusta, N., & Liu, Y. (2009). Three-dimensional boundary integral modeling of spontaneous earthquake sequences and aseismic slip. *Journal of Geophysical Research: Solid Earth*, *114*, B09303. doi: 10.1029/2008JB005934

Michel, S., Gualandi, A., & Avouac, J.-P. (2019). Similar scaling laws for earthquakes and Cascadia slow-slip events. *Nature*, *574*(7779), 522–526. doi: 10.1038/s41586-019-1673-6.

Noda, H., Lapusta, N., & Kanamori, H. (2013). Comparison of average stress drop measures for ruptures with heterogeneous stress change and implications for earthquake physics. *Geophysical Journal International*, *193*(3), 1691-1712. doi: 10.1093/gji/ggt074

Perfettini, H., Schmittbuhl, J., Rice, J. R., & Cocco, M. (2001). Frictional response induced by time-dependent fluctuations of the normal loading. *Journal of Geophysical Research: Solid Earth*, *106*(B7), 13455-13472. doi: 10.1029/2000JB900366

Radiguet, M., Cotton, F., Vergnolle, M., Campillo, M., Walpersdorf, A., Cotte, N., & Kostoglodov, V. (2012). Slow slip events and strain accumulation in the Guerrero gap, Mexico. *Journal of Geophysical Research: Solid Earth*, *117*, B04305. doi: 10.1029/2011JB008801.

Rubin, A. M., & Ampuero, J.-P. (2005). Earthquake nucleation on (aging) rate and state faults. *Journal of Geophysical Research: Solid Earth*, *110*, B11312. doi: 10.1029/2005JB003686.

Takagi, R., Uchida, N., & Obara, K. (2019). Along-strike variation and migration of long-term slow slip events in the western Nankai subduction zone, Japan. *Journal of Geophysical*

Research: Solid Earth, *124*(4), 3853–3880. doi: 10.1029/2019JB018037.

Wallace, L. M. (2020). Slow slip events in New Zealand. *Annual Review of Earth and Planetary Sciences*, *48*, 175–203. doi: 10.1146/annurev-earth-071719-055104.